Microporous and Mesoporous Materials 345 (2022) 112276

Contents lists available at ScienceDirect

Microporous and Mesoporous Materials

journal homepage: www.elsevier.com/locate/micromeso

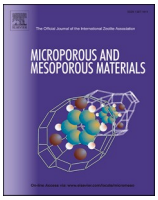

A non-doped microporous titanosilicate for bimodal adsorption-photocatalysis based removal of organic water pollutants

Ayomi S. Perera [a,*], Patrick M. Melia [a], Reece M.D. Bristow [a], James D. McGettrick [b], Richard J. Singer [a], Joseph C. Bear [a], Rosa Busquets [a]

[a] Kingston University London, Faculty of Science, Engineering and Computing, Kingston Upon Thames, KT1 2EE, UK
[b] SPECIFIC IKC, Materials Research Centre, College of Engineering, Swansea University, Bay Campus, Fabian Way, Swansea, SA1 8EN, UK

ARTICLE INFO

Keywords:
Photocatalysis
TiO2 alternative
Advanced oxidation
Water treatment
Porous adsorbent

ABSTRACT

Access to clean drinking water is limited for millions around the world and lead to dire health and economic ramifications, particularly in developing nations. This study explores a recyclable, low-cost, non-doped, microporous titanosilicate for effective removal of organic water pollutants. Rhodamine B was utilized as a modal pollutant to explore and optimize the activity of the titanosilicate, which evidently occurred *via* an adsorption and subsequent photocatalytic degradation based bimodal mechanism. The novel titanosilicate has high surface area (S_{BET} of 468 m^2/g), is microporous (~1.3 nm pore diameter), achieved *via* a surfactant templating technique. Its' physicochemical properties were characterised using FTIR, Raman, BET, SEM, PXRD and XPS. The photocatalytic activity of the material was studied under a solar simulator *via* time dependent UV–vis absorption measurements. The material showed 97% removal of Rhodamine B (5 mg/L) within 3 h, and outperformed nanosized titanium dioxide (anatase:rutile 4:1), the most conventionally used photocatalyst in tertiary water treatment. Interestingly, the titanosilicate displayed a dual mechanism of pollutant removal: an initial rapid removal of 59% due to adsorption during a 30 min equilibrating step in the dark, followed by near complete removal within 3 h. Additionally, a >90% efficiency of Rhodamine B removal by the titanosilicate catalyst was achieved consistently throughout 4 cycles, demonstrating its ability for regeneration and reusability. Such activity has not been previously reported in non-doped or non-composite titanosilicates, and opens up pathways to efficient, low-cost water treatment materials, consisting only of environmentally benign raw materials and synthetic procedures.

1. Introduction

Water pollution due to organic contaminants such as pesticides, antibiotics, dyes, plasticisers and pharmaceuticals is a growing concern around the world [1–5]. Developing countries in particular suffer grim environmental, health and economic consequences from pollution of surface and ground water, as a result of increased industrial production and usage of organic pollutants. These issues are unfortunately intensified by poor wastewater treatment capacities within such countries [6,7]. It therefore becomes imperative to develop affordable yet effective technologies that can remove these contaminants in a sustainable manner. Recent advances in decontamination of surface water include adsorption with activated carbons [3,8]; membrane techniques [9]; biological treatment [10]; and advanced oxidation methods, among others [11,12]. Photocatalysis is one such technique that is gaining prominence as a potentially effective water purification tool [13]. Sunlight driven photocatalytic degradation of organic contaminants has several advantages over other competing technologies, including providing complete mineralisation of contaminants, minimising waste and not requiring additional energy or chemical input [14].

One candidate class of materials that encompass the above characteristics, along with other useful advantages are titanosilicates. They are a structurally diverse class of zeolite-derivative materials that are currently used industrially as heterogeneous catalysts for alkene oxidation [15,16], and adsorbents/ion exchange agents for water filtration [17–19]. Their excellent catalytic properties are derived from the isolated, tetrahedrally coordinated Ti^{4+} active site centres, embedded within a silica matrix [20]. Titanosilicates also show photoactivity, reported to occur *via* highly dispersed titanium oxide species found within its structure [21], which were subsequently identified to be

* Corresponding author.
E-mail address: a.perera@kingston.ac.uk (A.S. Perera).

https://doi.org/10.1016/j.micromeso.2022.112276
Received 18 July 2022; Received in revised form 1 October 2022; Accepted 7 October 2022
Available online 12 October 2022

Ti^{4+} centres with tetrahedral coordination [22,23], now known to consist of -Ti-O-Si- linkages (unlike the -Ti-O-Ti- linkages found in TiO_2 which have octahedral geometry). Titanosilicates can be synthesised to have zeolite framework structures with highly customizable pore networks to target high product selectivity or reagent conversion depending on the desired reaction, which is a key advantage over TiO_2 [22,24]. Moreover, titanosilicates have displayed superior photocatalytic activity and selectivity compared to bulk TiO_2 [25], due to increased charge transfer and stabilization of photoactive species within their semiconductor framework [21,26]. These properties can be utilized for organic contaminant degradation, providing advanced avenues for the degradation of a myriad of organic contaminants. Notably, titanosilicates could become an alternative to TiO_2, which has been banned from use in food in Europe due to their suspected carcinogenicity in humans [27] – a trend that would likely expand on to water treatment.

Studies investigating titanosilicates as photocatalysts for the degradation of organic contaminants are scarce, compared to those focused on conventional heterogeneous catalysis. The ones that do, with activities comparable or surpassing TiO_2, often include either titanosilicates doped with toxic metals [26], or made into composite materials, such as with graphitic carbon nitride [28,29]. These extra components can be expensive and they are typically produced *via* hydrothermal synthesis, which requires heating at high temperatures over long periods of time, further adding to the cost of production. As a result, after three decades of promising research, titanosilicates are yet to surpass TiO_2 as commercially and industrially viable photocatalysts, particularly in water purification, despite having superior activity. It is therefore, imperative to focus research on developing cost effective, environmentally benign, yet efficient categories of titanosilicates for applications in advanced photocatalysis.

With the above goal in mind, this study was aimed to explore another well-known property of titanosilicates – adsorption, to be used in conjunction with photocatalytic ability, in order to enhance their capability in removal of organic impurities for applications in water treatment. Recent research has indicated a trend towards development of novel titanosilicates as adsorbents for removal of organic impurities, heavy metals and radioactive pollutants from water [28–32]. However, the preparation cost and use of non-environmentally benign reagents/-conditions on doped and nanocomposite titanosilicates in such works will likely prevent their use in real-world applications. The current study intended to address such drawbacks by development of non-doped, non-composite titanosilicates with high porosity and optimal active site concentration as key strategies in advancing sustainable Ti-based photocatalyst design. Templating with a surfactant/oil mixture was investigated as a cost-effective, facile technique to improve material porosity. This method has successfully been used previously to develop various types of titanosilicates with a wide range of structural properties and advanced pore structures to catalyse industrially relevant reactions [24,33,34].

Herein we outline the development of a new microporous titanosilicate (MiTS) in microbead morphology, without utilisation of any organic/inorganic dopants. Through the obtained results and analysis, we demonstrate that this material has potential relevance within the existing water treatment infrastructure, due to its ability to effectively remove organic contaminants, along with high recyclability, cost-effectiveness and environmental compatibility.

2. Experimental

2.1. Materials

The chemicals used for the preparation of the MiTS microbeads were tetraethyl orthosilicate (TEOS, 98%), Ti(IV) *n*-butoxide (97%), kerosene (b.p. 180–230 °C), Span® 80 (for synthesis), HNO_3 and ethanol (99.8%) purchased from Sigma-Aldrich Ltd. Rhodamine B (>95%), purchased from Alfa Aesar, was used in the degradation studies. Ultrapure water (15 MΩ·cm) was obtained with an ELGA Purelab system and used in all experiments.

2.2. Preparation of microporous titanosilicate microbeads

The microporous titanosilicate microbeads (MiTS) were prepared using an oil-water emulsion –mediated surfactant templating, adapted from Perera et al. [24], and modified to achieve high porosity. Initially, 1 mL of Ti(IV) *n*-butoxide (97%) was added dropwise to 30 mL of ultrapure water at 4 °C whilst stirring. The prepared $Ti(OH)_4$ precipitate was washed with ultrapure water and separated *via* filtration, before dissolving in 4 mL of 4 M HNO_3, producing the $TiO(NO_3)_2$ species. The active $TiO(NO_3)_2$ specie was stirred vigorously together with 6.6 mL of TEOS (98%) and 2 mL ethanol for 30 min before the microbead formation. The titanosilicate mixture was added to a mixture of 26.1 g kerosene and 7.9 g Span 80, and homogenized with a Heidolph RZR 1 homogeniser, at 2000 rpm for 2 h, at 80 °C. The beads were washed and vacuum-filtered with ultrapure water and acetone before drying at 50 °C under vacuum for 2 h. The beads were then calcined in a tube furnace (Carbolite Gero CWF 1200) at 750 °C for 6 h using a heating rate of 1 °C min^{-1}. The as prepared MiTS beads were stored in a desiccator and dried overnight at 50 °C under vacuum before use.

2.3. Characterisation

The titanosilicate microbeads were characterised using SEM, FTIR, Raman, PXRD, XPS and N_2 adsorption/desorption isotherms. For SEM analysis, the titanosilicate microbeads was mounted on specimen stubs fitted with adhesive carbon pads, sputter-coated with gold-palladium and examined using a Zeiss Evo50 (Oxford Instruments, Cambridge, UK) scanning electron microscope, where micrographs were obtained at an acceleration voltage of 20 kV. FTIR analysis was conducted with a Nicolet iS5 spectrometer with an iD1 transmission attachment (Thermo Scientific, UK). The analysis consisted of 20 scans with a resolution of 1 cm^{-1}. Raman spectra were obtained *via* a Renishaw InVia system (UK) along 100-1500 cm^{-1} with a green laser. PXRD analysis was conducted on a Bruker-AXS diffractometer, model D-8, using Cu K α radiation ($\lambda = 1.54184$ Å). N_2 adsorption-desorption isotherms were carried out at 77 K using a BELSORP-miniII porosimeter (MicrotracBEL, Japan). The titanosilicate microbeads were degassed for 24 h at 150 °C before isotherm measurements. The specific surface area (S_{BET}) was calculated using the standard BET (Brunauer-Emmett-Teller) model [35] and the BJH (Barrett-Joyner-Halenda) and MP/NLDFT models were used for pore characterisation. Total pore volume, V_p, was estimated at $P/P_0 \sim 0.99$, where P and P_0 denote equilibrium pressure and saturation pressure of N_2 at 77 K respectively.

XPS analysis was carried out on the microbeads after synthesis and after use to determine the composition, active Ti^{4+} site stability and degree of Rhodamine B degradation. X-ray Photoelectron Spectroscopy (XPS) was performed on a Kratos Axis Supra. Wide scans were collected in triplicate for each sample with a pass energy of 160 eV, with a monochromated Al Kα X-ray source (AlKα at 15 mA and 225 W). High resolution scans, at 40 eV pass energy, were undertaken for the Ti2p (450–470 eV), O1s (523–543 eV), C1s (278–298 eV) and Si2p (97–112 eV) regions, and fitted using the CasaXPS software package (Version 2.3.23rev1.1 K) using the default GL (mixed Gaussian-Lorentzian) lineshape and Shirley backgrounds unless otherwise stated. For the Ti2p and Si2p regions, doublet separation values of 5.7 eV[35] and 0.63 eV[36] respectively. The integral charge neutraliser was used throughout. For band-gap measurements, Ultra-violet visible (UV–Vis) spectroscopy was performed in diffuse reflectance mode on a Shimadzu UV–vis 2600 spectrophotometer equipped with an integrating sphere. A few mg of sample was pressed between two microscope slides for each measurement, and spectra were acquired over the 190–1200 nm range. The Kubelka-Munk function was applied to the data, with the band gap values determined using Tauc plots (Fig. 4 and S5).

2.4. Photocatalytic degradation of Rhodamine B

The Rhodamine B degradation studies were carried out within a 250 mL beaker using a 100 mL solution of 5 mg/L Rhodamine B in deionized water (15 MΩ) and 100 mg of the titanosilicate. A solar simulator (Newport, Oriel LCS-100, USA) was used to provide the simulated sunlight irradiation and was maintained at 7 inches (i.e., 178 mm) above the surface of the solution to replicate the intensity and spectrum of 1 sun, corresponding to AM1.5, or 1 kW/m^2. The AM1.5G spectral correction filter was used in order to achieve a light output to closely match the total (i.e., direct and diffuse) solar spectrum on the Earth's surface, at a zenith angle of 48.2° (ASTM 892). This generates a Class A irradiance spectrum suitable for photovoltaic cell testing. The solution containing the titanosilicate beads was stirrer under moderate conditions to ensure the equal contact of titanosilicate surface with the Rhodamine B solution. Aliquots (4 ml) were taken at various time intervals, centrifuged for 3 min at 3500 rpm, before analysis using UV–vis (Jenway 7315 Spectrophotometer, UK). After the measurement, the 4 mL aliquot was recombined using a vortex stirrer and returned to the beaker. A dark control (containing the catalyst) and light control (not containing the catalyst) were also conducted under the same conditions. Rhodamine B degradation was carried out over 4 cycles to investigate catalyst recyclability. The titanosilicate beads were recovered after each cycle through centrifugation and were kept in the dark and dried overnight before the subsequent cycle. The volume of solution was kept proportional to the mass of titanosilicate material remaining after each cycle during recycling experiments. The lamp height was also adjusted accordingly. For comparison purposes, the exact same experiments under simulated sunlight and in the dark were conducted with TiO_2 nanopowder (from US Nano, TX, USA) which was a 4:1 mixture of anatase and rutile with a 4 nm particle diameter.

Radical scavenging experiments were accomplished using the same Rhodamine B degradation procedure as described above, except with the addition of 1.0 mM *para*-benzoquinone (PBQ), and 1.0% (v/v) of isopropanol (IPA) to detect $O_2\bullet^-$, and •OH radicals, respectively, according to procedures from Fang et al. [36].

3. Results and discussion

3.1. Characterisation of microporous titanosilicate microbeads

Physicochemical characterisation of the MiTS material was performed with SEM, Raman, FTIR, PXRD, BET and XPS.

The SEM results (Fig. 1 A) show clustered microbeads, which are approximately 20–30 μm in diameter. Whilst most of the microbeads are isolated and spherical, some amalgamation of material in the form of a fusion of beads are evident. SEM micrographs also show micron sized pores, suggesting the presence of the oil/surfactant templating mixture prior to calcination, leaving behind a complex mesoporous/microporous structure, which will shift (in this case, to a predominantly microporous structure) based on homogenizing conditions, similar to previous reports [24,33].

The titanosilicate Raman spectrum (Fig. 1 B) showed prominent peaks at 960 nm and at 1107 nm, which are typical of Ti–O–Ti symmetric and asymmetric stretching, respectively [37]. This was compared against a commercial TiO_2 (anatase: rutile 4:1) which did not show the above two peaks but showed characteristic anatase bands at 144 nm, 395 nm (shoulder), 530 nm, 635 nm (broad) and rutile bands at 245 nm, 450 nm and 615 nm [38,39]. These peaks were not discernible on the titanosilicate spectrum, however, two broad shoulders at 140 nm and 450 nm were visible and likely correspond to silica phases [40] within the titanosilicate, in accordance with previous reports [24]. FTIR spectrum for the titanosilicate (Fig. 1 C) showed peaks at 945 cm^{-1} indicative of the Ti–O–Si asymmetric stretching, characteristic of

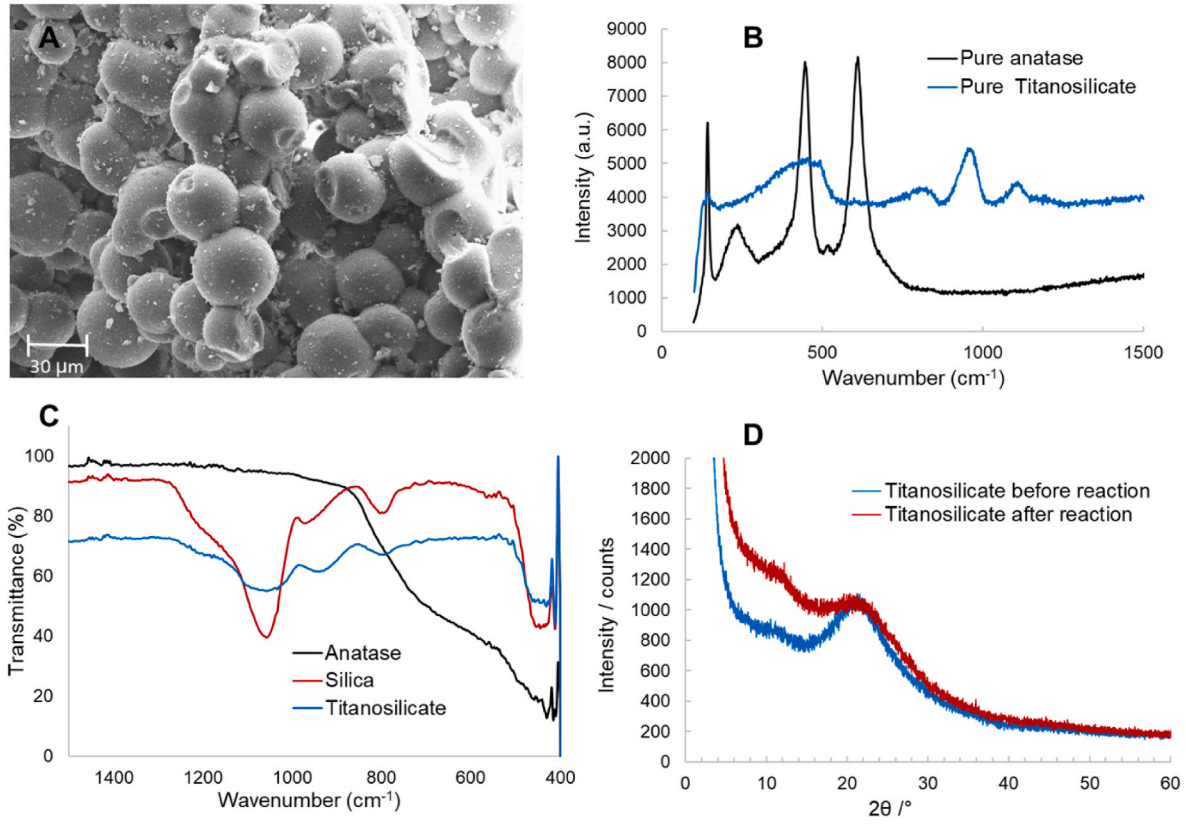

Fig. 1. Characterisation of titanosilicate microbeads. A - Scanning electron micrograph of titanosilicate beads, B - Raman spectra for anatase and titanosilicate, C - FTIR spectra for anatase, silica and titanosilicate, D – X-Ray Diffraction data for titanosilicate before and after photocatalytic reaction with Rhodamine B.

titanosilicates. Additionally, peaks at 1070 cm^{-1} for typical Si–O–Si asymmetric stretching and at 804 cm^{-1} for the O–Si–OH bending mode indicated the presence of the silica matrix, that were comparable to the reference SiO_2 sample spectrum and evidence the silica matrix present within the titanosilicate framework [24,33]. Anatase peaks seen in the commercial sample were not visible in the titanosilicate FTIR spectrum. The fingerprint region of the titanosilicate had a broad peak at ~460 nm corresponding to the analogous silica reference peak, indicating silica bending mode [41]. The PXRD results (Fig. 1 D) suggest an amorphous crystal structure [24], both before and after use, indicating the robustness of the material.

The pore structure of the titanosilicate microbeads generated *via* surfactant templating and subsequent calcination at 750 °C for removal of the oil/surfactant phase [33], was analysed *via* BET porosimetry. The size and volume of the pores were characterized *via* the BET (Brunauer-Emmett-Teller) and BJH (Barrett-Joyner-Halenda) methods respectively (Fig. 2 A and B). N_2 adsorption/desorption isotherms indicated that the titanosilicate microbeads had an S_{BET} surface area of 468 m^2/g, total pore volume of 0.459 cm^3/g and an average pore diameter of ~1.3 nm, with a predominantly microporous structure. The adsorption-desorption isotherms and BJH plots of the material both before and after its use as a photocatalyst, indicated that the majority of the material's pore and surface characteristics are retained after one reaction cycle (S_{BET} 418 m^2/g) with a slight increase to the degree of mesoporosity (average pore diameter ~2 nm) after use. This may be due to these pores becoming unblocked through use or relative disintegration of micropores into larger pores due to the mechanical impact of magnetic stirring of the titanosilicate beads over several catalytic cycles. Therefore, use of this material could be further optimised through immobilisation on a solid support, thus eliminating their mechanical breakdown and improving catalyst lifespan, which is currently under investigation in our laboratory.

3.2. Adsorption-photocatalysis based removal of Rhodamine B from water: A bimodal mechanism

Rhodamine B (Fig. 3 A) was utilized as a model pollutant to study the dual effects of adsorption-photocatalysis based removal from water with the novel titanosilicate (MiTS). Due to its high UV–vis absorbance, water solubility and polarity, Rhodamine B is an ideal candidate to study the targeted dual effect of MiTS on pollutant removal. However, it has a size of ~1.5–1.79 nm (depending on dimension side) [42], which hinders its ability to reach certain micropores within the titanosilicate structure. Thus, strong adsorption onto titanosilicate surface becomes an important factor in its degradation with the MiTS material discussed herein. The experiments were conducted in deionized water with a 5 mg/L initial concentration of Rhodamine B, for accurate quantification of the bimodal-mechanism. The main absorbance of Rhodamine B occurred at a maximum of 554 nm, the intensity of which was monitored to detect and quantify its removal from the water medium (Fig. 3 B). There were no new by-product peaks discernible *via* UV–vis during the 3-h reaction time, indicating that degradation products formed did not contain any chromophores or large conjugated molecular fragments (ESI Figure S1). The minor peaks present in the beginning of the reaction (*i.e.*, at 521 nm, 355 nm, 314 nm and 216 nm) were all degraded over time. This observation is in accordance with previous reports on photocatalytic degradation of Rhodamine B. [43,44]. Enhancement of light absorbance along 200–300 nm range with time does indicate that the fused microspheres of the titanosilicate catalyst maybe broken down into smaller fragments, which can easily be suspended in solution and typically absorb light in this range [24]. This was verified *via* SEM analysis of used catalyst, which indicated that the microspheres had partially fragmented during the reaction (ESI Figure S2).

Simulated sunlight generated *via* a solar simulator with irradiation intensity equivalent of 1 sun (or AM1.5, or 1 kW/m^2) was used to evaluate the photocatalytic efficiency of the titanosilicate against Rhodamine B removal. The changes in Rhodamine B concentration were monitored *via* UV–vis spectroscopy (Fig. 3 C). Three types of experiments were conducted with the MiTS material in order to assess the extent of both adsorption and photocatalysis on Rhodamine B removal: 1) control without the catalyst in light, 2) with catalyst in the dark, 3) with catalyst under irradiation. The concentration of Rhodamine B did not show any significant change without the titanosilicate catalyst, in the control experiment with irradiation, indicating that Rhodamine B does not degrade by sunlight alone. However, during the light experiment, the initial homogenizing step (t = −30 min–0 min, in the dark) indicated a drastic 59% reduction of Rhodamine B concentration in solution indicating significant adsorption onto the microporous titanosilicate, followed by 88% within 60 min, 94% within 120, and finally 97% in 180 min wit irradiation. Interestingly, during the dark experiment with catalyst, an identical level of adsorption was evident during the −30 min initial homogenizing step, followed by significant levels of Rhodamine B reduction within the 3 h, with a final value of 86%. Thus, the impact of adsorption during the process was evident. Commercial TiO_2 consisting of 4 nm diameter particles of anatase: rutile 4:1 mixture was also studied and was compared against the titanosilicate. This material did not show any adsorption during the −30 min homogenizing step and its overall Rhodamine B removal after the 3-h reaction time was comparable to that of the titanosilicate (Fig. 3 C).

The C/C_0 normalised data graph gives further insight into the impact of adsorption on the process of Rhodamine B removal (Fig. 3 D). Once represented in this manner, impact of the initial adsorption seen during the -30-0 min homogenizing step is essentially removed from the data, and the process of photocatalysis becomes clearer. Hence, the differences between light and dark experiments become prominent for MiTS-based removal of Rhodamine B. Moreover, the commercial TiO_2 appear to be the superior material based on photocatalysis alone. However, the MiTS would be a better option in application in real life water purification as the 4 nm particle size of commercial TiO_2 could escape from treatment units and would risk contamination of water. In contrast, the 20–30 μm size the MiTS particles are a safer option to for water filters. Moreover, it is a non-doped material, which can match the best

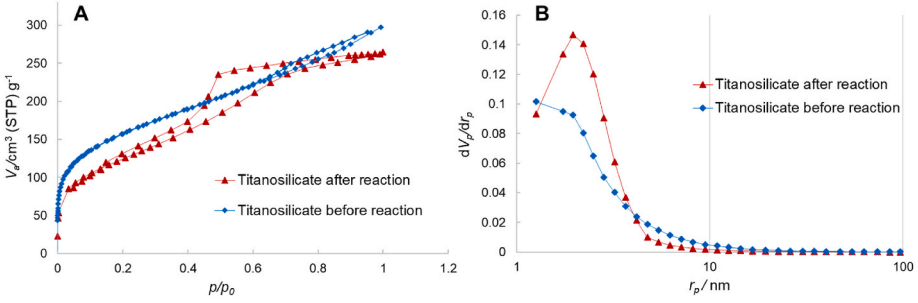

Fig. 2. A – N_2 adsorption-desorption isotherms of titanosilicate microbeads before and after use indicating a microporous structure before reaction and a shift towards mesoporosity after reaction, B – their respective BJH plots, confirming an increase in average pore diameter after reaction.

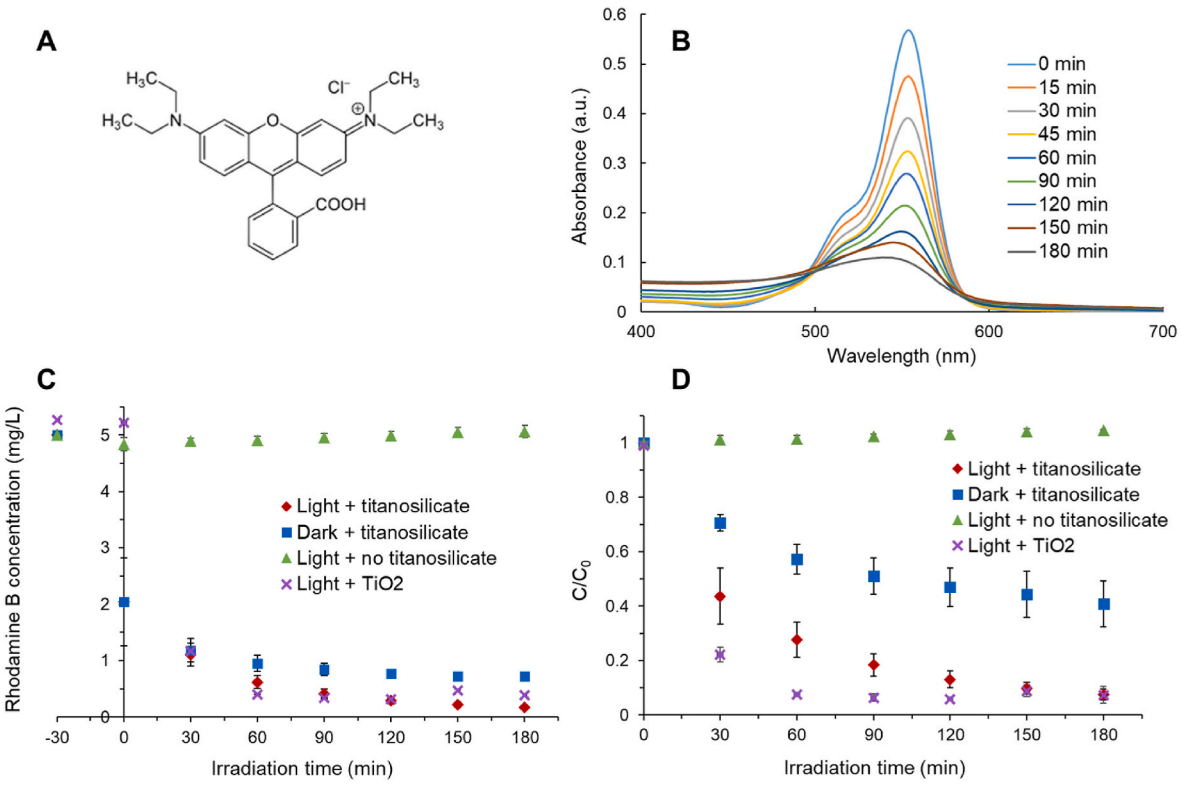

Fig. 3. Demonstration of photocatalytic activity of titanosilicates against Rhodamine B. A - Chemical structure of Rhodamine B; B – UV–vis absorbance of Rhodamine B with time under photocatalysis with titanosilicate; C - degradation of Rhodamine B concentration against time with titanosilicate and commercial TiO_2 (anatase: rutile 4:1). The −30 to 0 min step indicates homogenizing in the dark leading to significant and fast adsorption of dye on the porous titanosilicate catalyst; D - normalised graph of Rhodamine B degradation against time, where C_0 is the starting concentration of Rhodamine B and C is the Rhodamine B concentration after its removal against time.

conventionally known photocatalyst TiO_2. Additionally, the MiTS catalyst are capable of removing pollutants in the dark and during poor light conditions due to adsorption, whereas the TiO_2 tested above showed no such activity (ESI Figure S3). The favourable particle size and non-use of expensive dopants together with superior adsorbent-photocatalytic activity, paves a new path for advanced water purification using titanosilicates.

The considerable adsorption of Rhodamine B onto the titanosilicate catalyst that takes place during this bimodal-mechanism-based photocatalytic reaction (5 mg of Rhodamine B per 100 mg of titanosilicate) plays a key role in its kinetic progression. Considering typical Langmuir-Hinshelwood kinetics for a porous catalyst and one reactant reaction where adsorption is significant [45,46], the reaction appears to fit within pseudo first order kinetics (ESI Figure S4). When the −30 min homogenizing step where high adsorption takes place was included, the rate constants were found to be 0.023 $mgl^{-1}min^{-1}$ within the first hour, 0.019 $mgl^{-1}min^{-1}$ within the second hour and 0.016 $mgl^{-1}min^{-1}$ within the total 3-h reaction time. However, if the latter were to be eliminated, the rates change to 0.020 $mgl^{-1}min^{-1}$, 0.016 and 0.014 $mgl^{-1}min^{-1}$ within the first, second and third hours respectively, representing 13.0%, 15.8% and 12.5% drops in respective rates. Considering this discrepancy and the dual mechanism, a further inspection of factors that influence kinetic parameters of photocatalytic degradation needed to be considered. The rates of photocatalytic reactions are found to be dependent on light intensity, reactant concentration, pH of the medium, temperature and catalyst concentration [47,48], all of which are kept constant in our study. Since our light source is kept at optimum height to the reaction mixture to receive maximum intensity, and that the reaction is small scale, it can be assumed that the local light intensity experienced by the mixture is high and uniform. In such a case the photocatalyst is found to behave as a typical heterogeneous catalyst and not be influenced by kinetics related to the flux of absorbed photons on its surface [47]. This theory however, considers that all available active sites are exposed to light, which may not be the case for our 20–30 μm sized catalyst, which has pores consisting predominantly of ~1.3 nm. Hence, the calculated reaction rates should be taken as an approximation on reaction kinetics. Nevertheless, they shed light into the potential application of the material in water purification with regards to its effectivity and stability. It must be noted that experiments conducted in the dark are now particularly useful in determining the effect of adsorption-based removal of Rhodamine B.

Diffuse reflectance studies of the titanosilicate followed by the Kubelka-Munk analysis, indicated a direct band gap of 3.63 eV for the material (Fig. 4). This is higher than the typical band gap value reported for commercial P25 semiconductor, which is 3.2 eV E_g. However it is closer to higher end of TiO_2 prepared by sol–gel method (3.4–3.1 eV), which are considered the best semiconductor options for environmental

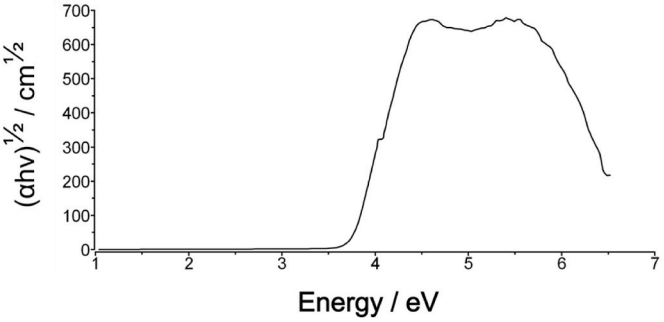

Fig. 4. Band gap energy data generated *via* Kubelka-Munk analysis of diffuse-reflectance UV–vis data for the titanosilicate.

applications [49]. It is important to note that the titanosilicate reported herein was synthesised *via* a sol-gel method [24]. The 4 nm TiO_2 reference used herein indicated a band gap of 3.18 eV (ESI Figure S5), which is considerably lower than the titanosilicate. Despite the higher band gap, the tianosilicate gives very close Rhodamine B degradation results to that of the TiO_2 nanopowder, further evidencing the importance and advantage of adsorption that occur during this process.

3.3. Radical quenching experiments

In order to gain insight into the mechanism of photocatalytic degradation of Rhodamine B, experiments were conducted in the presence of *para*-benzoquinone (PBQ) and isopropanol (IPA), which are known to quench radicals $O_2\bullet^-$ and •OH respectively. It was apparent that both PBQ and IPA inhibited the degradation of Rhodamine B significantly, compared to the experiments conducted without them, and under the same irradiation conditions (Fig. 5). Thus, it was apparent that both $O_2\bullet^-$ and •OH radicals are produced during the photocatalytic degradation of Rhodamine B at the conditions given under visible light irradiation, in accordance with previous studies. [36,50]. Intriguingly, it was evident that the process of adsorption of Rhodamine B onto the catalyst, which occurs predominantly during the initial −30 to 0 min homogenizing step, is inhibited more by IPA than PBQ (Fig. 5 A). However, at the end of the 3-h reaction time, the experiments with both scavenger compounds yielded the same results as the experiments conducted in the dark, where only adsorption takes place. The overall Rhodamine B degradation by the titanosilicate after 3 h for IPA and PBQ were found to be 86% and 88% respectively, which were close to the 86% removal shown by the experiments in the dark. Once the data was normalised by plotting C/C_0 to remove the effect of the initial adsorption step (Fig. 5 B), it appeared that •OH scavenger IPA had more of an impact on reaction inhibition than the $O_2\bullet^-$ scavenger PBQ. In reality however, since adsorption does play an integral part of the catalyst's mechanism, the concentration vs. time graph should be considered to for a more accurate depiction of progression this reaction catalysed *via* our titanosilicate.

3.4. Recyclability

The MiTS photocatalyst was recycled over 4 cycles in order to monitor recovery and recyclability. For light based photocatalytic reaction cycles (Fig. 6 A), only 5% loss of activity was evident after the 3-h reaction time between cycles 1 and 2, indicating the robustness of the material. There were no significant differences in Rhodamine B removal evident among cycles 2–4 (>0.5%). The dark control data and indicates the adsorptive capacity of the titanosilicate for the dye (Fig. 6 B). The adsorption capacity decreases over time, when four consecutive recycling experiments are conducted in the dark. However, this would not be an issue in real life day-night usage, as the adsorbed dye is degraded over time (Fig. 7) – after turning pink upon adsorption of the dye (after 3 h equilibration) the MiTS return to its original white colour after further irradiation (19 h). This further indicates the potential for regeneration and reuse of the MiTS material within multiple cycles.

3.5. Elemental analysis: further mechanistic insights

Further to Raman and IR analyses, the composition of the titanosilicate samples were analysed by X-ray photoelectron spectroscopy (XPS). Survey scans (taken over 0–1350 keV) revealed the samples were composed of titanium, silicon and oxygen as expected for as-synthesised titanosilicate samples. It was also evident that the calcining step removed nearly all carbon contamination. During the photocatalytic experiments, titanosilicate samples were isolated after 3 and 19 h by centrifugation, before drying *in vacuo* and analysis by XPS. The amount of carbon in the sample increased, and as XPS is a surface-sensitive technique, this is good evidence for dye adsorption to the surface of the titanosilicates. The average elemental composition in the titanosilicates show some variation before and after reactions (Table 1, ESI Figure S6). Samples X, Y and Z correspond to the as-synthesised titanosilicate powder (X), after 3 h of Rhodamine B photocatalytic degradation (Y) and after 19 h of Rhodamine B photocatalytic degradation (Z). (These labels correspond to the high-resolution C1s scans given in Fig. 7 C.)

The compositions listed in Table 1 (and indeed supported by the C1s scans in Fig. 7) show a marked increase in the amount of carbon in the sample as soon as the photocatalytic degradation of Rhodamine B was underway. The carbon content increase from 6.1 atom % in the as-synthesised titanosilicate sample (X) to 20.9 atom % after 3 h of photodegradation of Rhodamine B. Due to the way in which the samples were prepared for XPS (*i.e.* centrifugation before drying), any adsorbed material (*i.e.* dye) would be included in the analysis. This accounts for the significantly higher proportion of carbon in Sample Y when compared to Samples X and Z (after degradation was complete). This observation supports the notion that surface adsorption of Rhodamine B is a key part of the bimodal mechanism of pollutant degradation in the MiTS titanosilicate material. After 19 h of reaction however, the carbon content has significantly reduced, indicating a return to the surface chemistry of the as-synthesised material. This is a favourable factor for considerations in recycling and reusing of the material.

The model used to fit high resolution scans of the Ti2p region consisted of 2 components, with a more oxidised component (at higher binding energy) attributed to a titanosilicate TiO_2/SiO_2 or tetrahedrally coordinated environment, similar to that found in literature [51,52] and confirmed by us in a previous study [24]. This likely corresponds to the Ti–O–Si bonds in the active sites of the titanosilicate. The more reduced component has a similar binding energy to titanium in a TiO_2 or octahedrally coordinated environment [53], and this coupled with the more oxidised component, forms the basic structure of the titanosilicate

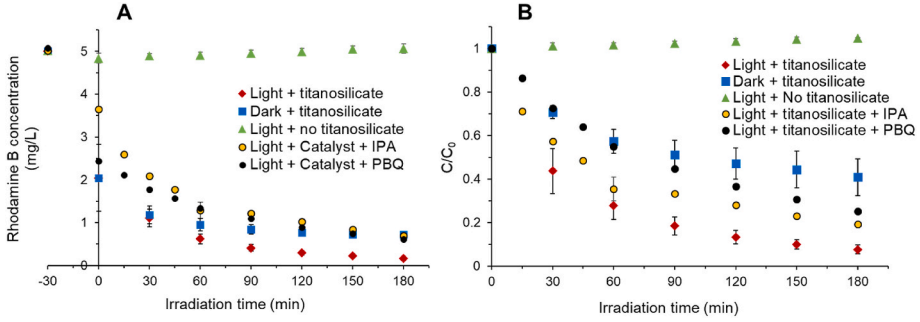

Fig. 5. Proof of photocatalytic mechanism of Rhodamine B degradation with the titanosilicate, under the presence of radical quencher compounds isopropanol (IPA) and *para*-benzoquinone (PBA). A – Rhodamine B concentration against time, B – normalised graph of Rhodamine B degradation against time, where C_0 is the starting concentration of Rhodamine B and C is the Rhodamine B concentration after its removal against time.

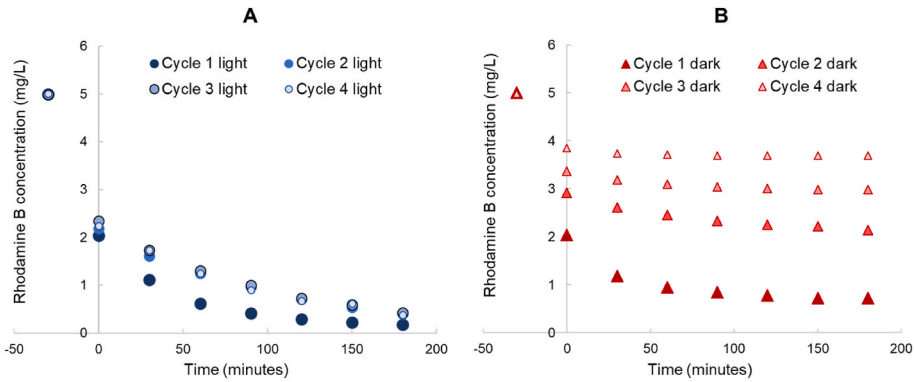

Fig. 6. Recyclability of the MiTS titanosilicate photocatalyst with respect to Rhodamine B degradation over four reaction cycles; A - under simulated sunlight and B - in the dark.

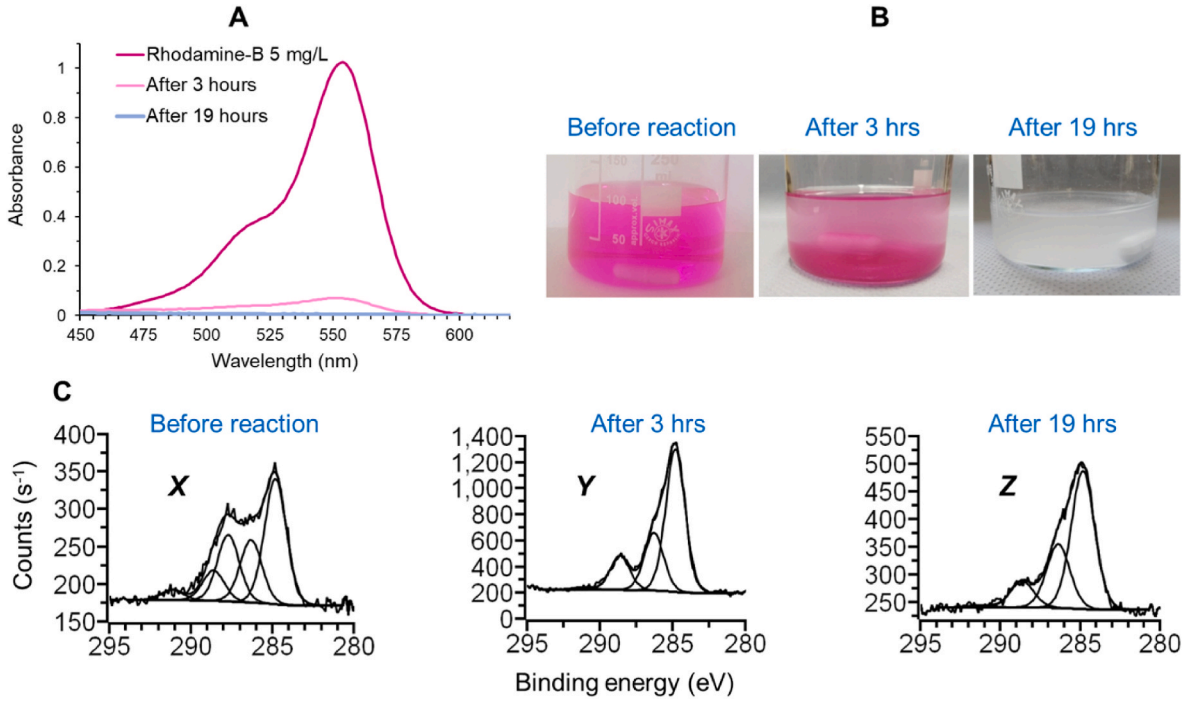

Fig. 7. A: UV–vis spectra of typical photocatalytic degradation of Rhodamine B, which indicates the gradual loss of the peak at *ca.* 560 nm over time. The dispersions were centrifuged prior to UV–vis analysis to avoid any scattering effects from the titanosilicate powder. B: Photographs corresponding to the photocatalytic degradation prior to reaction, after 3 h and after 19 h. C: High-resolution C1s XPS spectra showing the changing carbon environments. Note the increase in intensity of the C1s environment after 3 h, indicating surface adsorption of Rhodamine B, with a sharp loss of intensity after 19 h of reaction time.

Table 1
Average atom % compositions calculated from XPS of the as-synthesised titanosilicate samples (X), after 3 h of photocatalytic degradation of Rhodamine B (Y) and after 19 h of reaction time (Z). The Si:Ti ratio is given in the final column.

Average composition (Atom %)					
Sample identifier	C1s	O1s	Si2p	Ti2p	Si:Ti ratio
X	6.10	75.2	16.5	2.30	7.5
Y	20.9	64.8	13.2	1.10	11.7
Z	10.7	71.9	14.9	2.60	5.8

Table 2
The changing ratio of the fitted Ti2p environments in our fitted model for Samples X, Y and Z. The "TiO_2" peak has a lower binding energy (ca. 458.7 eV for $Ti2p_{3/2}$) and the higher binding energy "TiO_2/SiO_2" peak (*ca.* 459.6 eV for $Ti2p_{3/2}$). Ratios are calculated from the area of the $Ti2p_{3/2}$ peaks.

Concentration (Atom %)			
Sample Identifier	TiO_2 peak	TiO_2/SiO_2 peak	Ratio
X	1.13	1.37	0.830
Y	0.735	0.675	1.09
Z	2.26	0.553	4.08

material with active catalytic Ti–O–Si sites in the vicinity of Ti–O–Ti phases. During the reaction, the ratio of the two environments changed, presumably due to occupation of the catalytically active sites by the Rhodamine B dye (Table 2).

The increase in the ratio of the TiO_2:TiO_2/SiO_2 peaks after 19 h is in contrast to the decrease in the amount of carbonaceous material seen in Table 1 and Fig. 5. These data indicated that the surface availability of the oxidised TiO_2/SiO_2 component changes post reaction rather than returning to the ratio seen in Sample X. This could possibly be due to the partial collapse of the pore structure during the reaction (see Fig. 2), which made certain sites inaccessible during XPS analysis. In addition,

the apparent change in TiO_2/SiO_2 quantity does not seem to affect the photocatalytic activity or the rate of degradation in repeat cycles (see Fig. 6). The material retains its ability to remove Rhodamine B effectively for four consecutive catalytic cycles. The role in adsorption processes may play a key role in maintaining this activity as a way to mitigate possible changes in the chemical structure of the material, thus enhancing its' robustness. These interesting observations warrant further investigation, along with degradation studies on prevalent organic water pollutants such as pesticides, antibiotics etc., but is beyond the scope of the present 'proof-of-concept' study.

4. Conclusions

A novel titanosilicate was prepared in microbead morphology of 20–30 μm diameter, *via* an oil-water emulsion based surfactant-templating technique, without the addition of any dopants. The synthesised material was found to have a microporous structure with ~1.3 nm pores and a high BET surface area of 468 m^2/g. The isolated, tetrahedrally coordinated Ti^{4+} sites within the prepared materials, responsible for its catalytic activity, were confirmed with FTIR, Raman and XPS, and found to be stable throughout its use. The titanosilicate was found to be effective in the sunlight driven degradation of the bulky, model organic pollutant Rhodamine B, degrading over 97% of it within a first 3-h cycle. This activity was comparable to commercial TiO_2 nanopowder (4 nm, anatase:rutile 4:1). However, the titanosilicates being micron-sized would be a far safer option for water treatment as larger particles would be less likely to leach out of filtration units. The titanosilicate also appeared to be recyclable and reusable indicating >90% removal of Rhodamine B over 4 reaction cycles, obtained consistently. Adsorption was found to play a major role in the materials' ability to remove Rhodamine B, accounting for 59% of its removal during an initial −30 min homogenizing step, in the dark, and a subsequent 86% removal within 3 h in the dark. These findings suggest that a bimodal adsorption-photocatalysis based mechanism takes place, allowing for fast and sustained removal of organic pollutants under simulated sunlight. Due to this activity, process cost-effectiveness and environmental benignity of raw materials used, this material has potential to be applied in tertiary water treatment. Further studies must test the ability to degrade a wider range of emerging contaminants to determine its scope of application.

Funding sources

The authors gratefully acknowledge the funding provided by UKRI HEFCE-GCRF grant and the Department of Chemical and Pharmaceutical Sciences at Kingston University.

CRediT authorship contribution statement

Ayomi S. Perera: Writing – review & editing, Writing – original draft, Supervision, Project administration, Methodology, Investigation, Funding acquisition, Conceptualization. **Patrick M. Melia:** Writing – review & editing, Methodology, Investigation, Formal analysis. **Reece M.D. Bristow:** Writing – review & editing, Methodology, Formal analysis. **James D. McGettrick:** Writing – review & editing, Formal analysis. **Richard J. Singer:** Supervision, Methodology, Formal analysis. **Joseph C. Bear:** Writing – review & editing, Methodology, Data curation. **Rosa Busquets:** Writing – review & editing, Supervision, Project administration.

Declaration of competing interest

The authors declare that they have no known competing financial interests or personal relationships that could have appeared to influence the work reported in this paper.

Data availability

Data will be made available on request.

Acknowledgements

The authors gratefully acknowledge the contributions from Mr Richard Giddens for his assistance in conducting the SEM experiments, Mr Simon Crust for assistance with Raman spectroscopy, Dr Andreas Kafizas of Imperial College London for help with solid-state UV/Vis measurements and Mr Owen Lawler for technical support with FTIR analysis.

Appendix A. Supplementary data

Supplementary data to this article can be found online at https://doi.org/10.1016/j.micromeso.2022.112276.

References

[1] M. Syafrudin, R.A. Kristanti, A. Yuniarto, T. Hadibarata, J. Rhee, W.A. Al-Onazi, T. S. Algarni, A.H. Almarri, A.M. Al-Mohaimeed, Pesticides in drinking water-A review, Int. J. Environ. Res. Publ. Health 18 (2) (2021) 468, https://doi.org/10.3390/ijerph18020468.
[2] M.-C. Danner, A. Robertson, V. Behrends, J. Reiss, Antibiotic pollution in surface fresh waters: occurrence and effects, Sci. Total Environ. 664 (2019) 793–804, https://doi.org/10.1016/J.SCITOTENV.2019.01.406.
[3] U. Shanker, M. Rani, V. Jassal, Degradation of hazardous organic dyes in water by nanomaterials, Environ. Chem. Lett. 15 (4) (2017) 623–642, https://doi.org/10.1007/s10311-017-0650-2.
[4] O.M. Ogunbanwo, P. Kay, A.B. Boxall, J. Wilkinson, C.J. Sinclair, R.A. Shabi, A. E. Fasasi, G.A. Lewis, O.A. Amoda, L.E. Brown, High concentrations of pharmaceuticals in a Nigerian river catchment, Environ. Toxicol. Chem. 41 (3) (2022) 551–558, https://doi.org/10.1002/etc.4879.
[5] M.J. Whelan, C. Linstead, F. Worrall, S.J. Ormerod, I. Durance, A.C. Johnson, D. Johnson, M. Owen, E. Wiik, N.J.K. Howden, T.P. Burt, A. Boxall, C.D. Brown, D. M. Oliver, D. Tickner, Is water quality in British rivers "better than at any time since the end of the industrial revolution", Sci. Total Environ. 843 (2022), 157014 https://doi.org/10.1016/j.scitotenv.2022.157014.
[6] K. Balakrishna, A. Rath, Y. Praveenkumarreddy, K.S. Guruge, B. Subedi, A review of the occurrence of pharmaceuticals and personal care products in Indian water bodies, Ecotoxicol. Environ. Saf. 137 (2017) 113–120, https://doi.org/10.1016/j.ecoenv.2016.11.014.
[7] L.C. Pereira, A.O. de Souza, M.F. Franco Bernardes, M. Pazin, M.J. Tasso, P. H. Pereira, D.J. Dorta, A perspective on the potential risks of emerging contaminants to human and environmental health, Environ. Sci. Pollut. Res. Int. 22 (18) (2015) 13800–13823, https://doi.org/10.1007/s11356-015-4896-6.
[8] Z. Li, J. Li, Z. Guo, L.C. Campos, Investigation of metaldehyde removal by powdered activated carbon from different water samples, Environ. Sci. Water Res. Technol. 6 (5) (2020) 1432–1444, https://doi.org/10.1039/C9EW00962K.
[9] W.T. Vieira, M.B. de Farias, M.P. Spaolonzi, M.G.C. da Silva, M.G.A. Vieira, Removal of endocrine disruptors in waters by adsorption, membrane filtration and biodegradation. A review, Environ. Chem. Lett. 18 (4) (2020) 1113–1143, https://doi.org/10.1007/s10311-020-01000-1.
[10] N.A. Zhou, H.L. Gough, Enhanced biological trace organic contaminant removal: a lab-scale demonstration with bisphenol A-degrading bacteria sphingobium sp. BiD32, Environ. Sci. Technol. 50 (15) (2016) 8057–8066, https://doi.org/10.1021/acs.est.6b00727.
[11] L.V. Nguyen, R. Busquets, S. Ray, A.B. Cundy, Graphene oxide-based degradation of metaldehyde: effective oxidation through a modified fenton's process, Chem. Eng. J. 307 (2017) 159–167, https://doi.org/10.1016/j.cej.2016.08.052.
[12] E. Kudlek, Decomposition of Contaminants of Emerging Concern in Advanced Oxidation Processes, Water, 2018, https://doi.org/10.3390/w10070955.
[13] R. Quesada-Cabrera, C. Sotelo-Vazquez, J.C. Bear, J.A. Darr, I.P. Parkin, Photocatalytic evidence of the rutile-to-anatase electron transfer in titania, Adv. Mater. Interfac. 1 (6) (2014), 1400069, https://doi.org/10.1002/admi.201400069.
[14] S.K. Loeb, P.J.J. Alvarez, J.A. Brame, E.L. Cates, W. Choi, J. Crittenden, D. D. Dionysiou, Q. Li, G. Li-Puma, X. Quan, D.L. Sedlak, T. David Waite, P. Westerhoff, J.-H. Kim, The technology horizon for photocatalytic water treatment: sunrise or sunset? Environ. Sci. Technol. 53 (6) (2019) 2937–2947, https://doi.org/10.1021/acs.est.8b05041.
[15] US-4410501-A @ Pubchem.Ncbi.Nlm.Nih.Gov.
[16] D.R.C. Huybrechts, L. De Bruycker, P.A. Jacobs, Oxyfunctionalization of alkanes with hydrogen peroxide on titanium silicalite, Nature 345 (6272) (1990) 240–242, https://doi.org/10.1038/345240a0.
[17] L. Lv, G. Tsoi, X.S. Zhao, Uptake equilibria and mechanisms of heavy metal ions on microporous titanosilicate ETS-10, Ind. Eng. Chem. Res. 43 (24) (2004) 7900–7906, https://doi.org/10.1021/ie0498044.

[18] D.M. Poojary, R.A. Cahill, A. Synthesis Clearfield, Crystal structures, and ion-exchange properties of a novel porous titanosilicate, Chem. Mater. 6 (12) (1994) 2364–2368, https://doi.org/10.1021/cm00048a024.
[19] M.A. Roberts, G. Sankar, J.M. Thomas, R.H. Jones, H. Du, J. Chen, W. Pang, R. Xu, Synthesis and structure of a layered titanosilicate catalyst with five-coordinate titanium, Nature 381 (6581) (1996) 401–404, https://doi.org/10.1038/381401a0.
[20] A.S. Perera, M.-O. Coppens, Titano-silicates: highlights on development, evolution and application in oxidative catalysis, in: Catalysis, vol. 28, The Royal Society of Chemistry, 2016, pp. 119–143, https://doi.org/10.1039/9781782626855-00119, vol. 28.
[21] Z. Juan, Z. Dishun, Y. Liyan, L. Yongbo, Photocatalytic oxidation dibenzothiophene using TS-1, Chem. Eng. J. 156 (3) (2010) 528–531, https://doi.org/10.1016/j.cej.2009.04.032.
[22] M. Anpo, H. Yamashita, K. Ikeue, Y. Fujii, S.G. Zhang, Y. Ichihashi, D.R. Park, Y. Suzuki, K. Koyano, T. Tatsumi, Photocatalytic reduction of CO2 with H2O on Ti-MCM-41 and Ti-MCM-48 mesoporous zeolite catalysts, Catal. Today 44 (1) (1998) 327–332, https://doi.org/10.1016/S0920-5861(98)00206-5.
[23] G.D. Lee, S.K. Jung, Y.J. Jeong, J.H. Park, K.T. Lim, B.H. Ahn, S.S. Hong, Photocatalytic decomposition of 4-nitrophenol over titanium silicalite (TS-1) catalysts, Appl. Catal. Gen. 239 (1) (2003) 197–208, https://doi.org/10.1016/S0926-860X(02)00389-7.
[24] A.S. Perera, P. Trogadas, M.M. Nigra, H. Yu, M.-O. Coppens, Optimization of mesoporous titanosilicate catalysts for cyclohexene epoxidation via statistically guided synthesis, J. Mater. Sci. 53 (10) (2018) 7279–7293, https://doi.org/10.1007/s10853-018-2057-2.
[25] H. Yamashita, Y. Ichihashi, M. Anpo, M. Hashimoto, C. Louis, M. Che, Photocatalytic decomposition of NO at 275 K on titanium oxides included within Y-zeolite cavities: the structure and role of the active sites, J. Phys. Chem. 100 (40) (1996) 16041–16044, https://doi.org/10.1021/jp9615969.
[26] S. Uma, S. Rodrigues, I.N. Martyanov, K.J. Klabunde, Exploration of photocatalytic activities of titanosilicate ETS-10 and transition metal incorporated ETS-10, Microporous Mesoporous Mater. 67 (2) (2004) 181–187, https://doi.org/10.1016/j.micromeso.2003.11.003.
[27] European Commision, Goodbye E171: the EU bans titanium dioxide as a food additive. https://ec.europa.eu/newsroom/sante/items/732079/en. (Accessed 18 July 2022).
[28] A.K. Adepu, R. Anumula, V. Narayanan, Photocatalytic degradation of rhodamine B over a novel mesoporous titanosilicate/g-C3N4 nanocomposite under direct sunlight irradiation, Microporous Mesoporous Mater. 247 (2017) 86–94, https://doi.org/10.1016/j.micromeso.2017.03.046.
[29] A.K. Adepu, V. Katta, V. Narayanan, Synthesis, characterization, and photocatalytic degradation of rhodamine B dye under sunlight irradiation of porous titanosilicate (TS)/Bismuth vanadate (BiVO4) nanocomposite hybrid catalyst, New J. Chem. 41 (6) (2017) 2498–2504, https://doi.org/10.1039/C7NJ00071E.
[30] Y.K. Kim, S. Kim, Y. Kim, K. Bae, D. Harbottle, J.W. Lee, Facile one-pot synthesis of dual-cation incorporated titanosilicate and its deposition to membrane surfaces for simultaneous removal of Cs+ and Sr2+, Appl. Surf. Sci. 493 (2019) 165–176, https://doi.org/10.1016/j.apsusc.2019.07.008.
[31] H. Liu, A. Yonezawa, K. Kumagai, M. Sano, T. Miyake, Cs and Sr removal over highly effective adsorbents ETS-1 and ETS-2, J. Mater. Chem. 3 (4) (2015) 1562–1568, https://doi.org/10.1039/C4TA06170E.
[32] K. Popa, C.C. Pavel, Radioactive wastewaters purification using titanosilicates materials: state of the art and perspectives, Desalination 293 (2012) 78–86, https://doi.org/10.1016/j.desal.2012.02.027.
[33] A.S. Perera, J.K. Cockcroft, P. Trogadas, H. Yu, N. Kapil, M.-O. Coppens, Titanium (IV)-Induced cristobalite formation in titanosilicates and its potential impact on catalysis, J. Mater. Sci. 54 (1) (2019) 335–345, https://doi.org/10.1007/s10853-018-2869-0.
[34] K. Egeblad, C.H. Christensen, M. Kustova, C.H. Christensen, Templating mesoporous zeolites, Chem. Mater. 20 (3) (2008) 946–960, https://doi.org/10.1021/cm702224p.
[35] S.J. Gregg, K.S.W. Sing, Adsorption, Surface Area and Porosity, second ed., Academic Press, London, 1995.
[36] S. Fang, K. Lv, Q. Li, H. Ye, D. Du, M. Li, Effect of acid on the photocatalytic degradation of rhodamine B over G-C3N4, Appl. Surf. Sci. 358 (2015) 336–342, https://doi.org/10.1016/j.apsusc.2015.07.179.
[37] G. Ricchiardi, A. Damin, S. Bordiga, C. Lamberti, G. Spanò, F. Rivetti, A. Zecchina, Vibrational structure of titanium silicate catalysts. A spectroscopic and theoretical study, J. Am. Chem. Soc. 123 (46) (2001) 11409–11419, https://doi.org/10.1021/ja010607v.
[38] F.D. Hardcastle, Raman spectroscopy of titania (TiO2) nanotubular water-splitting catalysts, J. Ark. Acad. Sci. (2011).
[39] S. Challagulla, K. Tarafder, R. Ganesan, S. Roy, Structure sensitive photocatalytic reduction of nitroarenes over TiO2, Sci. Rep. 7 (1) (2017) 8783, https://doi.org/10.1038/s41598-017-08599-2.
[40] E. Berrier, C. Zoller, F. Beclin, S. Turrell, M. Bouazaoui, B. Capoen, Microstructures and structural properties of Sol−Gel silica foams, J. Phys. Chem. B 109 (48) (2005) 22799–22807, https://doi.org/10.1021/jp053089+.
[41] T.N. Tran, T. Van Anh Pham, M.L. Phung Le, T.P. Thoa Nguyen, V.M. Tran, Synthesis of amorphous silica and sulfonic acid functionalized silica used as reinforced phase for polymer electrolyte membrane, Adv. Nat. Sci. Nanosci. Nanotechnol. 4 (4) (2013), 45007, https://doi.org/10.1088/2043-6262/4/4/045007.
[42] J. Canning, G. Huyang, M. Ma, A. Beavis, D. Bishop, K. Cook, A. McDonagh, D. Shi, G.-D. Peng, M.J. Crossley, Percolation diffusion into self-assembled mesoporous silica microfibres, Nanomaterials (2014), https://doi.org/10.3390/nano4010157.
[43] T. Liu, L. Wang, X. Lu, J. Fan, X. Cai, B. Gao, R. Miao, J. Wang, Y. Lv, Comparative study of the photocatalytic performance for the degradation of different dyes by ZnIn2S4: adsorption, active species, and pathways, RSC Adv. 7 (20) (2017) 12292–12300, https://doi.org/10.1039/C7RA00199A.
[44] H. Yang, J. Yang, Photocatalytic degradation of rhodamine B catalyzed by TiO2 films on a capillary column, RSC Adv. 8 (22) (2018) 11921–11929, https://doi.org/10.1039/C8RA00471D.
[45] G.W. Roberts, C.N. Satterfield, Effectiveness factor for porous catalysts. Langmuir-hinshelwood kinetic expressions, Ind. Eng. Chem. Fundam. 4 (3) (1965) 288–293, https://doi.org/10.1021/i160015a009.
[46] T. Sauer, G. Cesconeto Neto, H.J. José, R.F.P. Moreira, Kinetics of photocatalytic degradation of reactive dyes in a TiO2 slurry reactor, J. Photochem. Photobiol. Chem. 149 (1) (2002) 147–154, https://doi.org/10.1016/S1010-6030(02)00015-1.
[47] J.Z.A. Bloh, Holistic approach to model the kinetics of photocatalytic reactions, Front. Chem. 7 (2019) 128, https://doi.org/10.3389/fchem.2019.00128.
[48] B.O. Burek, D.W. Bahnemann, J.Z. Bloh, Modeling and optimization of the photocatalytic reduction of molecular oxygen to hydrogen peroxide over titanium dioxide, ACS Catal. 9 (1) (2019) 25–37, https://doi.org/10.1021/acscatal.8b03638.
[49] R. López, R. Gómez, Band-gap energy estimation from diffuse reflectance measurements on sol–gel and commercial TiO2: a comparative study, J. Sol. Gel Sci. Technol. 61 (1) (2012) 1–7, https://doi.org/10.1007/s10971-011-2582-9.
[50] K. Nagaveni, M.S. Hegde, N. Ravishankar, G.N. Subbanna, G. Madras, Synthesis and structure of nanocrystalline TiO2 with lower band gap showing high photocatalytic activity, Langmuir 20 (7) (2004) 2900–2907, https://doi.org/10.1021/la035777v.
[51] S. Contarini, P.A.W. van der Heide, A.M. Prakash, L. Kevan, Titanium coordination in microporous and mesoporous oxide materials by monochromated X-ray Photoelectron spectroscopy and X-ray auger electron spectroscopy, J. Electron. Spectrosc. Relat. Phenom. 125 (1) (2002) 25–33, https://doi.org/10.1016/S0368-2048(02)00041-5.
[52] G. Moretti, A.M. Salvi, M.R. Guascito, F. Langerame, An XPS study of microporous and mesoporous titanosilicates, Surf. Interface Anal. 36 (10) (2004) 1402–1412, https://doi.org/10.1002/sia.1931.
[53] J.C. Bear, V. Gomez, N.S. Kefallinos, J.D. McGettrick, A.R. Barron, C.W. Dunnill, Anatase/rutile Bi-phasic titanium dioxide nanoparticles for photocatalytic applications enhanced by nitrogen doping and platinum nano-islands, J. Colloid Interface Sci. 460 (2015) 29–35, https://doi.org/10.1016/j.jcis.2015.08.027.